



HAL
open science

On the Study of Interference and their Localization in the Time-Frequency Plane

Sylvain Meignen, Thomas Oberlin

► **To cite this version:**

Sylvain Meignen, Thomas Oberlin. On the Study of Interference and their Localization in the Time-Frequency Plane. 2021. hal-03327526

HAL Id: hal-03327526

<https://hal.science/hal-03327526>

Preprint submitted on 27 Aug 2021

HAL is a multi-disciplinary open access archive for the deposit and dissemination of scientific research documents, whether they are published or not. The documents may come from teaching and research institutions in France or abroad, or from public or private research centers.

L'archive ouverte pluridisciplinaire **HAL**, est destinée au dépôt et à la diffusion de documents scientifiques de niveau recherche, publiés ou non, émanant des établissements d'enseignement et de recherche français ou étrangers, des laboratoires publics ou privés.

On the Study of Interference and their Localization in the Time-Frequency Plane

Sylvain Meignen, Thomas Oberlin

Abstract—In this paper, our goal is first to investigate the conditions for the separation of the modes making up multicomponent signals based on the analysis of the short-time Fourier transform. More precisely, we put forward necessary and sufficient conditions for the existence of ridges associated with the modes in the time-frequency plane. The focus is put on signals either made of purely harmonic modes or parallel linear chirps, for which we show that when the modes are strongly interfering in the time-frequency plane, the ridges no longer exist and are replaced by some structures called time-frequency bubbles. Based on a careful study of interference patterns, we show that the zeros of the spectrogram involved in these share very specific features, on which we found a new algorithm to determine interference locations based on the Delaunay triangulation of spectrogram zeros.

Index Terms—Time-frequency analysis, short-time Fourier transform, spectrogram zeros, Delaunay triangulation.

I. INTRODUCTION

The analysis of multicomponent signals (MCSs) using *time-frequency representations* (TFRs) has been the subject of intense research in the last few decades, since the modes making up a MCS are associated with specific regions around TF curves, called *ridges* [1], [2]. The locations of these ridges lead to estimates the *instantaneous frequencies* (IFs) of the modes [3], [4]. Among linear TFRs the most popular ones are the *short-time Fourier Transform* (STFT) and the *continuous wavelet transform* (CWT) while the most commonly used quadratic TFR is the spectrogram.

The quality of IF estimation from ridge extraction is tightly related to how well the modes are separated in the TF plane, namely to the choice of the analysis window in the case of spectrogram. Indeed, an inappropriate window choice results in mode interference. In that framework, optimal window length can be found by minimizing the Rényi entropy which is proved to be a good measure of the level of interference in the TF plane [5], [6]. However, even when one considers the TFR minimizing the Rényi entropy, there is no guarantee that the modes are not interfering in the TF plane. To improve mode separation for IF estimation, the so-called *adaptive short-time Fourier transform* (ASTFT) was introduced [7], [8] and recently adapted to the context of synchrosqueezing transform [9], [10]. Alternative techniques aiming at improving IF estimation from reassigned transform

[11] were also developed in [12], [13], the basic principle of these approaches being to disentangle the components at interference locations by modifying the reassignment process. Note that reassignment approaches are also very common to deal with overlapping transients, a situation frequently encountered in echolocation calls [14], [15]. In this regard, multi-taper approaches [16] result in significant improvement in terms of transient separation on that type of signals [17].

To adapt locally the window length to reduce interference, one often uses the argument that the sparsest representations should lead to the best IF estimation. Nevertheless, such an adaption is not necessary at each time instant to obtain good mode separation. To have an insight into where to modify the window length, an analysis of the TF interference pattern can be carried out. It was remarked in [18] that the TFR associated with the Gabor transform of the sum of two pure harmonic modes could exhibit so-called *time-frequency bubbles* (TFBs), consisting of circles of local maxima at the TF location of the two modes. Such structures were also observed in more complex situations [18]. In practice, TFBs arise when, at some time instant, two modes generate only a single maximum of the spectrogram. When TFBs are present, the estimation of the IF of the modes based on ridge extraction is no longer possible. Though in [18] some elements were given to explain when such TFBs occurred, a clear mathematical analysis was lacking. In the present paper, our first goal is thus to bridge that gap, putting forward a necessary and sufficient condition for the existence of TFBs when the signal is made of two pure harmonic modes and when the TFR is the spectrogram. Then, we show how to extend these conditions to the case of the sum of two parallel linear chirps.

More generally, the spectrogram of close modes can be viewed as a continuum from separate ridges to TFBs, the latter corresponding to the highest level of interference. For IF estimation based on ridge detection, it is crucial to determine where interference occur in the TF plane, because even a low interference level can reduce drastically the quality of IF estimation from TF ridges. For that purpose, we analyze interference patterns, and show that these involve local maxima, zeros and saddle points of the spectrogram. Based on this study, we propose a novel algorithm to localize interference in the TF plane based on Delaunay triangulation of the zeros of the spectrogram involved in interference patterns.

The motivation for using the zeros of the spectrogram can be found in the pioneering work by Flandrin [19]. In that paper, the zeros of the spectrogram of Gaussian white noise were studied, and further investigated in [20]. The conclusions of these papers were that, on the one hand,

S. Meignen is with the Jean Kuntzmann Laboratory, University Grenoble Alpes and CNRS 5225, Grenoble 38401, France (email:sylvain.meignen@univ-grenoble-alpes.fr), while T. Oberlin is with ISAE-SUPAERO, Université de Toulouse, 31055 Toulouse CEDEX 4, France. This work is supported by the ANR-ASCETE project with grant number ANR-19-CE48-0001-01.

the spectrogram zeros tend not to clutter and, on the other hand, they cannot be too far one from another. Based on this last remark, a new technique using Delaunay triangulation of spectrogram zeros was proposed to separate the noise from the signal in the spectrogram [21]. The rationale supporting the algorithm proposed in that paper was basically that the signal corresponded to zero-free regions, and thus the surrounding zeros generated triangles with long edges in the Delaunay triangulation of the spectrogram zeros. Thus, the criterion chosen to separate the triangles related to noise from those corresponding to the signal was based of the analysis of the edge length in the triangulation. We here propose to develop a variant to this approach to localize interference in the TF plane. More precisely, we study in details the nature of the triangles surrounding the zeros involved in the Delaunay triangulation and then found our algorithm to localize interference on that analysis.

The paper is organized as follows. In the following section, we introduce the notation that we will use throughout the paper. Then, we state the main theoretical contributions regarding the existence of TFBS, studying successively the case of a signal made either of two pure harmonic modes or of parallel linear chirps. Finally, we propose a novel technique to localize mode interference in the TF plane based on the Delaunay triangulation of spectrogram zeros.

II. NOTATION

Considering a signal $f \in L^1(\mathbb{R}) \cap L^2(\mathbb{R})$ and a real window $h \in L^\infty(\mathbb{R}) \cap L^2(\mathbb{R})$, the (modified) short-time Fourier transform (STFT) is defined as:

$$V_f^h(t, \eta) = \int_{\mathbb{R}} f(\tau) h(\tau - t) e^{-2i\pi(\tau - t)\eta} d\tau, \quad (1)$$

the spectrogram being the square modulus of V_f^h . In the sequel, we are going to study the interference between the modes of a multicomponent signal (MCS), defined as the superposition of P AM-FM components:

$$f(t) = \sum_{p=1}^P f_p(t) \text{ with } f_p(t) = A_p(t) e^{2i\pi\phi_p(t)}, \quad (2)$$

in which the *instantaneous amplitudes* (IAs) $A_p(t)$ are positive, as well as the *instantaneous frequencies* (IFs) $\phi_p'(t)$. We further assume that the IFs are sorted in decreasing order, namely $\phi_{p+1}'(t) > \phi_p'(t)$ for all t .

III. FREQUENCY DOMAIN INTERFERENCE

In this section, we first investigate the existence of TFBS when the signal is the sum of two pure harmonic modes. We then explain how the obtained results can be extended to the case of two parallel linear chirps. More precisely, we show that the existence of these TFBS is related to that of extrema of the spectrogram. For our study, we will use the Gaussian window $h(t) = e^{-\pi \frac{t^2}{\sigma^2}}$ to define the STFT, because with that choice analytical results can be derived.

A. Existence of TFBS in the Case of the Sum of the Two Pure Harmonic Signals

Let $f(t) = f_1(t) + f_2(t)$ with $f_1(t) = Ae^{i2\pi\xi_1 t}$ and $f_2(t) = e^{i2\pi\xi_2 t}$, where $\xi_1 < \xi_2$. For such a signal, one has $V_{f_1}^h(t, \eta) = \hat{h}(\eta - \xi_1) Ae^{i2\pi\xi_1 t} = \sigma Ae^{i2\pi\xi_1 t} e^{-\pi(\eta - \xi_1)^2 \sigma^2}$ and $V_{f_2}^h(t, \eta) = \sigma e^{i2\pi\xi_2 t} e^{-\pi(\eta - \xi_2)^2 \sigma^2}$ and thus:

$$|V_f^h(t, \eta)|^2 = \sigma^2 (A^2 e^{-2\pi\sigma^2(\eta - \xi_1)^2} + e^{-2\pi\sigma^2(\eta - \xi_2)^2} + 2Ae^{-\pi\sigma^2[(\eta - \xi_1)^2 + (\eta - \xi_2)^2]} \cos(2\pi(\xi_2 - \xi_1)t)) \quad (3)$$

which attains, considering η fixed, its maximum at $t_k = \frac{k}{\xi_2 - \xi_1}$, $k \in \mathbb{Z}$ for which:

$$|V_f^h(t_k, \eta)|^2 = \sigma^2 (Ae^{-\pi\sigma^2(\eta - \xi_1)^2} + e^{-\pi\sigma^2(\eta - \xi_2)^2})^2. \quad (4)$$

Studying $|V_f^h(t_k, \cdot)|^2$, where \cdot means we consider this variable, we get the following result.

Proposition III.1. $|V_f^h(t_k, \cdot)|^2$ has three extrema if and only if $\alpha := \sqrt{\frac{\pi}{2}} \sigma (\xi_2 - \xi_1) > 1$ and

$$|\log(A)| < 2\alpha\sqrt{\alpha^2 - 1} - \log\left(\frac{\alpha + \sqrt{\alpha^2 - 1}}{\alpha - \sqrt{\alpha^2 - 1}}\right) = 2\alpha\sqrt{\alpha^2 - 1} - 2 \operatorname{arccosh}(\alpha). \quad (5)$$

In any other case, $|V_f^h(t_k, \cdot)|^2$ has a unique extremum which is a maximum.

The proof is given in Appendix A. Note that one can easily show that the extrema are all in the interval $]\xi_1, \xi_2[$. If $A = 1$, remarking that $\log\left(\frac{\alpha + \sqrt{\alpha^2 - 1}}{\alpha - \sqrt{\alpha^2 - 1}}\right) = 2 \operatorname{arccosh}(\alpha)$ the condition to have three extrema reads:

$$2\alpha\sqrt{\alpha^2 - 1} - \log\left(\frac{\alpha + \sqrt{\alpha^2 - 1}}{\alpha - \sqrt{\alpha^2 - 1}}\right) > 0 \Leftrightarrow -\operatorname{arccosh}(\alpha) + \alpha\sqrt{\alpha^2 - 1} > 0. \quad (6)$$

As the function $-\operatorname{arccosh}(x) + x\sqrt{x^2 - 1}$ is strictly increasing on $[1, +\infty[$ and is zero at zero, the condition boils down to $\alpha > 1$.

Now, η being fixed, let us consider the time instants where $|V_f^h(t, \eta)|^2$ attains its minima which correspond to time $t = \tilde{t}_k = \frac{1/2 + k}{\xi_2 - \xi_1}$, $k \in \mathbb{Z}$, at which:

$$|V_f^h(\tilde{t}_k, \eta)|^2 = \sigma^2 (e^{-\pi\sigma^2(\eta - \xi_1)^2} - Ae^{-\pi\sigma^2(\eta - \xi_2)^2})^2. \quad (7)$$

Then, we have the following proposition regarding the number of extrema of $|V_f^h(\tilde{t}_k, \cdot)|^2$:

Proposition III.2. $|V_f^h(\tilde{t}_k, \cdot)|^2$ has a unique minimum inside the interval $[\xi_1, \xi_2]$, a unique maximum on the interval $]\xi_2, +\infty[$, and a unique maximum on the interval $]-\infty, \xi_1[$.

The proof is available in Appendix B. This can be generalized to other time instants than t_k and \tilde{t}_k in the case $A = 1$, since we have the following proposition.

Proposition III.3. If $A = 1$, $|V_f^h(t, \cdot)|^2$ has three extrema if and only if $\alpha = \sqrt{\frac{\pi}{2}} \sigma (\xi_2 - \xi_1)$ satisfies:

$$\alpha > \sqrt{\frac{1 + \cos(2\pi(\xi_2 - \xi_1)t)}{2}} \quad (8)$$

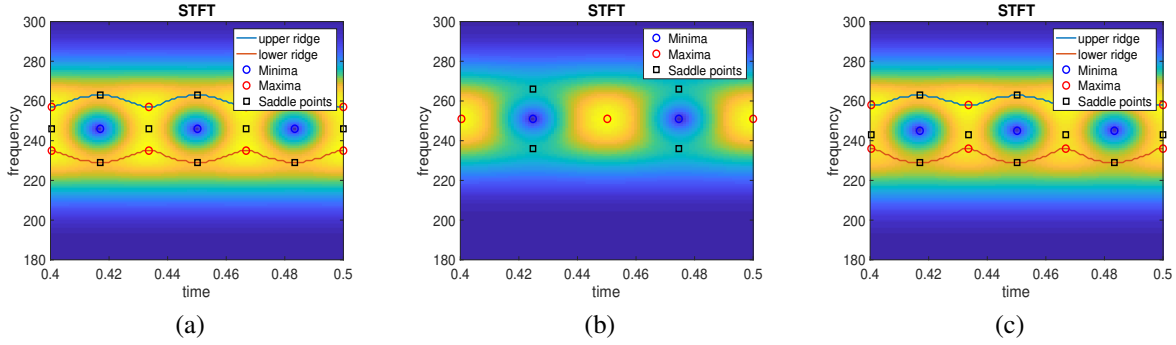


Fig. 1: (a): spectrogram of two parallel pure harmonic modes with the same amplitude, when there exists three extrema at each time instant (ridges are thus well defined); (b): spectrogram of two parallel pure harmonic modes exhibiting TFBs (ridges associated with each mode can no longer be defined); (c): same as (a) but when the pure harmonic modes have different amplitude (three extrema are still present but the symmetry no longer exists).

and one otherwise.

The proof is available in Appendix C. This can be generalized to any time t and any amplitude A through the following:

Proposition III.4. Assuming α is defined as in Proposition III.3, and defining $\gamma = \cos(2\pi(\xi_2 - \xi_1)t)$, $|V_f^h(t, \cdot)|^2$ has three extrema if and only if $\alpha > \sqrt{\frac{1+\gamma}{2}}$ and

$$|\log(A)| < -\operatorname{arccosh}(X_2) + 2\alpha^2 \frac{\sqrt{X_2^2 - 1}}{X_2 + \gamma}, \quad (9)$$

with $X_2 = \gamma(\alpha^2 - 1) + \alpha\sqrt{\gamma^2(\alpha^2 - 2) + 2}$. In any other case, $|V_f^h(t, \cdot)|^2$ has a unique extremum.

The proof is available in Appendix D. Note that when $\gamma = 1$, we get $X_2 = 2\alpha^2 - 1$, and then

$$\begin{aligned} -\operatorname{arccosh}(X_2) + 2\alpha^2 \frac{\sqrt{X_2^2 - 1}}{X_2 + 1} &= -\operatorname{arccosh}(X_2) + \sqrt{X_2^2 - 1} \\ &= -\operatorname{arccosh}(2\alpha^2 - 1) + 2\alpha\sqrt{\alpha^2 - 1} \quad (10) \\ &= -2\operatorname{arccosh}(\alpha) + 2\alpha\sqrt{\alpha^2 - 1} \end{aligned}$$

which is exactly the condition of Proposition III.1. Similarly, when $A = 1$ the right hand side of (9) is positive and the condition to have three extrema boils down to $\alpha > \sqrt{\frac{1+\gamma}{2}}$, which is the condition enounced in Proposition III.3.

Now, to finish this study we state a necessary and sufficient condition to have three extrema:

Proposition III.5. $|V_f^h(t, \cdot)|^2$ whatever t has three extrema if and only if $\alpha := \sqrt{\frac{\pi}{2}}\sigma(\xi_2 - \xi_1) > 1$ and

$$|\log(A)| < -2\operatorname{arccosh}(\alpha) + 2\alpha\sqrt{\alpha^2 - 1}. \quad (11)$$

In any other case there exists some time t where $|V_f^h(t, \cdot)|^2$ has a unique extremum.

The proof is given in Appendix E. This last proposition means that if the spectrogram has three extrema at t_k then it has three extrema at each time t . In that context, the existence of TFBs is related to the conditions of Proposition III.1 being not fulfilled. In such a case, each mode cannot be associated

with a ridge. To illustrate this, we consider the spectrogram of the sum of two pure harmonic modes with $A = 1$ such that the conditions of Proposition III.1 are fulfilled in Fig. 1 (a) and not in Fig. 1 (b), in which TFBs appear. Finally, in Fig. 1 (c), we consider the case $A \neq 1$ when the conditions of Proposition III.1 are fulfilled. We notice that the locations of the extrema of the spectrogram at time instants \tilde{t}_k , and in particular the locations of the zeros, are not much changed. But, this is not the case of the extrema locations at time t_k .

B. Existence of TFBs in the Case of two Parallel Linear Chirps

Our goal is now to extend the previous study to parallel linear chirps. We thus consider $f(t) = f_1(t) + f_2(t)$ with $f_1(t) = Ae^{2i\pi\phi_1(t)}$ and $f_2(t) = e^{2i\pi\phi_2(t)}$, with $\phi_1''(t) = \phi_2''(t) = C$ constant. It can be easily shown that in such a case one has:

$$\begin{aligned} |V_f^h(t, \eta)|^2 &= r^{-1} \left(A^2 e^{-\frac{2\pi\sigma^2(\eta - \phi_1'(t))^2}{1+C^2\sigma^4}} + e^{-\frac{2\pi\sigma^2(\eta - \phi_2'(t))^2}{1+C^2\sigma^4}} \right. \\ &\quad \left. + 2Ae^{-\pi\frac{\sigma^2[(\eta - \phi_1'(t))^2 + (\eta - \phi_2'(t))^2]}{1+C^2\sigma^4}} \cos(2\pi\phi(t, \eta)) \right), \quad (12) \end{aligned}$$

with $r = \sqrt{\frac{1}{\sigma^4} + C^2}$ and

$$\begin{aligned} \phi(t, \eta) &= \phi_2(t) - \phi_1(t) \\ &+ \frac{C\sigma^4}{1+C^2\sigma^4} (\phi_2'(t) - \phi_1'(t)) \left(\eta - \frac{\phi_2'(t) + \phi_1'(t)}{2} \right). \quad (13) \end{aligned}$$

Now, given a real number γ in $[-1, 1]$, let us consider the set of TF points (t, η) such that $\cos(2\pi\phi(t, \eta)) = \gamma$. These points are such that $\phi(t, \eta) = \frac{\arccos(\gamma)}{2\pi} + k = \beta_k$. As $\phi_1(t) = a_1t + \frac{C}{2}t^2$ and $\phi_2(t) = a_2t + \frac{C}{2}t^2$, we have that:

$$\begin{aligned} (a_2 - a_1) \left(t + \frac{C\sigma^4}{1+C^2\sigma^4} \left(\eta - \frac{a_1 + a_2 + 2Ct}{2} \right) \right) &= \beta_k \\ \Leftrightarrow t &= -C\sigma^4\eta + \frac{\beta_k(1+C^2\sigma^4) + \frac{(a_2^2 - a_1^2)C\sigma^4}{2}}{a_2 - a_1} \quad (14) \\ &\Leftrightarrow t = D\eta + B_k. \end{aligned}$$

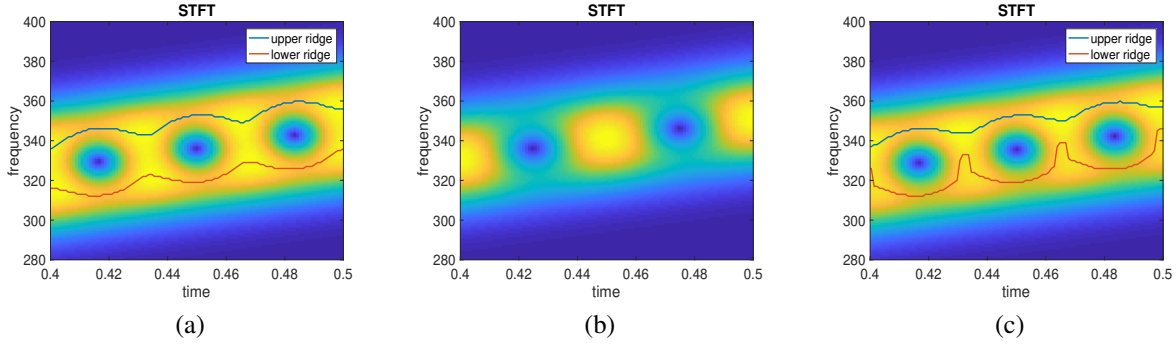


Fig. 2: (a): Spectrogram of two parallel linear chirps with the same amplitude, when there exists three extrema at each time instant in the direction D , the upper and lower ridges are also superimposed; (b): Spectrogram of two parallel linear chirps when TFBs are present (three extrema no longer exist in the direction D for each translation factor B_k , and ridge extraction is no longer possible); (c): same as (a) but when the linear chirps have different amplitude (three extrema are still present along the direction D).

From this, we deduce that

$$\begin{aligned} & |V_f^h(D\eta + B_k, \eta)|^2 = r^{-1} \\ & \left(A^2 e^{-\frac{2\pi\sigma^2(\eta - a_1 - C(D\eta + B_k))^2}{1+C^2\sigma^4}} + e^{-\frac{2\pi\sigma^2(\eta - a_2 - C(D\eta + B_k))^2}{1+C^2\sigma^4}} \right. \\ & \quad \left. + 2Ae^{-\pi\frac{\sigma^2[(\eta - a_1 - C(D\eta + B_k))^2 + (\eta - a_2 - C(D\eta + B_k))^2]}{1+C^2\sigma^4}} \gamma \right) \quad (15) \\ & = r^{-1} \left(A^2 e^{-2\pi\tilde{\sigma}^2(\eta - \frac{a_1 + CB_k}{1-CD})^2} + e^{-2\pi\tilde{\sigma}^2(\eta - \frac{a_2 + CB_k}{1-CD})^2} + \right. \\ & \quad \left. 2Ae^{-\pi\tilde{\sigma}^2[(\eta - \frac{a_1 + CB_k}{1-CD})^2 + (\eta - \frac{a_2 + CB_k}{1-CD})^2]} \gamma \right), \end{aligned}$$

with $\tilde{\sigma} = \frac{\sigma(1-CD)}{\sqrt{1+C^2\sigma^4}} = \sigma\sqrt{1+C^2\sigma^4}$. As the expression (15) is the same as (3) replacing σ by $\tilde{\sigma}$ and ξ_1 and ξ_2 respectively by $\frac{a_1 + CB_k}{1-CD}$ and by $\frac{a_2 + CB_k}{1-CD}$. This leads to the following properties

Proposition III.6. Assume (t, η) is evolving on the line $t = D\eta + B_k$ such that $\cos(2\pi\phi(t, \eta)) = 1$, then $|V_f^h(t, \eta)|^2$ has three extrema (two maxima and one minimum) along the line $t = D\eta + B_k$ if and only if:

$$\sqrt{\frac{\pi}{2}}\tilde{\sigma}(a_2 - a_1) > 1,$$

and a unique maximum in that interval otherwise.

The proof is the same as that of Proposition III.1. If we now consider the case $\gamma = -1$, we have the following property:

Proposition III.7. Assume (t, η) is on the line $t = D\eta + B_k$, such that $\cos(2\pi\phi(t, \eta)) = -1$, $|V_f^h(t, \eta)|^2$ always has, along the line $t = D\eta + B_k$, a unique minimum for $\eta \in [\frac{a_1 + CB_k}{1-CD}, \frac{a_2 + CB_k}{1-CD}]$, a unique maximum for $\eta \in]\frac{a_2 + CB_k}{1-CD}, +\infty[$, and a unique maximum in the interval $] -\infty, \frac{a_1 + CB_k}{1-CD}[$

The proof is the same as that of Proposition III.2. Going further we can prove that for any $\gamma \in [-1, 1]$:

Proposition III.8. If $A = 1$, $|V_f^h(t, \eta)|^2$ has three extrema along the line $t = D\eta + B_k$ if and only if $\alpha_C = \sqrt{\frac{\pi}{2}}\tilde{\sigma}(a_2 - a_1)$

satisfies:

$$\alpha_C > \sqrt{\frac{1+\gamma}{2}},$$

and one otherwise.

The proof of Proposition III.8 follows the same line as that of Proposition III.3. The arguments can be generalized to any A by adapting Proposition III.4 as follows:

Proposition III.9. Assuming α_C is defined as in Proposition III.8, and that $\gamma = \cos(2\pi\phi(t))$, $|V_f^h(t, \eta)|^2$ has three extrema along the line $t = D\eta + B_k$ if and only if $\alpha_C > \sqrt{\frac{1+\gamma}{2}}$ and

$$|\log(A)| < -\text{arccosh}(X_2) + 2\alpha_C^2 \frac{\sqrt{X_2^2 - 1}}{X_2 + \gamma}, \quad (16)$$

with $X_2 = \gamma(\alpha_C^2 - 1) + \alpha_C\sqrt{\gamma^2(\alpha_C^2 - 2) + 2}$. In any other case, $|V_f^h(t, \eta)|^2$ has a unique extremum along the line $t = D\eta + B_k$.

We finally state a necessary and sufficient condition to have three extrema along the direction D :

Proposition III.10. $|V_f^h(t, \eta)|^2$ has three extrema along the line $t = D\eta + B_k$ if and only if $\alpha_C := \sqrt{\frac{\pi}{2}}\tilde{\sigma}(a_2 - a_1) > 1$ and

$$|\log(A)| < -2\text{arccosh}(\alpha_C) + 2\alpha_C\sqrt{\alpha_C^2 - 1}. \quad (17)$$

In any other case, where $|V_f^h(t, \eta)|^2$ has a unique extremum along the line $t = D\eta + B_k$.

An illustration of this is given in Fig. 2 (a) where we display the spectrogram of two parallel linear chirps for which there always exist 3 extrema in the direction D , making ridge extraction tractable, then, in Fig. 2 (b), we display the case where there exists only one extremum in the direction D for some value of γ , and thus TFBs are present. Finally, in Fig. 2 (c) we display a case where there are still three extrema in the direction D but when A is no longer equal to 1. Note that, as the computation of saddle points involves the determination of the direction D , we do not display extrema in that case, but

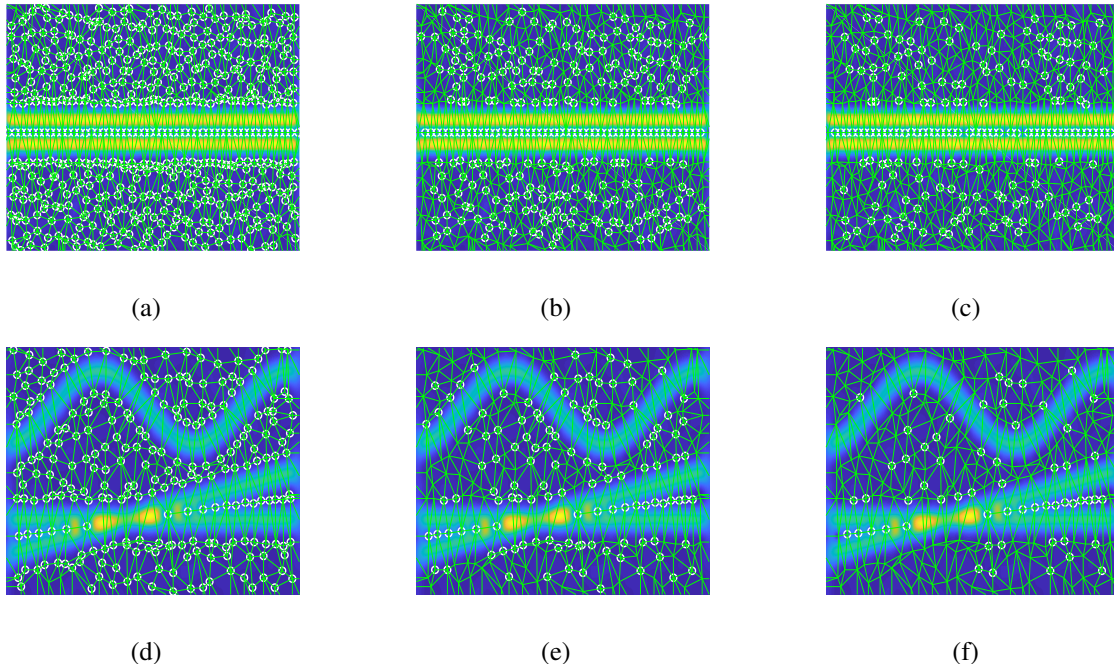


Fig. 3: (a): spectrogram of two interfering modes with DTSZ superimposed, the white circles correspond to vertices \mathbf{v} such that $I(\mathbf{v}, 30) \geq 1$ (input SNR = 20 dB); (b): same as (a) except the white circles correspond to vertices \mathbf{v} such that $I(\mathbf{v}, 30) \geq 4$; (c): same as (a) with $I(\mathbf{v}, 30) \geq 4$; (d): spectrogram of three interfering modes with DTSZ superimposed, the white circles correspond to vertices \mathbf{v} such that $I(\mathbf{v}, 30) \geq 1$ (input SNR = 20 dB); (e): same as (d) with $I(\mathbf{v}, 30) \geq 4$; (f): same as (d) with $I(\mathbf{v}, 30) \geq 5$.

the conclusion regarding the stability of the zeros observed in the case of two pure harmonic modes remains valid here.

IV. DETERMINATION OF THE INTERFERENCE REGIONS USING SPECTROGRAM ZEROS

A. Motivation for Using Spectrogram Zeros

The previous study tells us that when two modes are interfering, there always exist zeros at some time instants located between the IF of the modes, even when TFBs are present. On the contrary, as shown in the previous section, the number of local maxima of the spectrogram involved in interference patterns may vary both in terms of their number and locations. Furthermore, we numerically notice that the saddle points are very unstable in noisy situations. For these reasons, to localize interference in the TF plane we are not going to directly use the saddle points or the maxima of the spectrogram, but rather the zeros generated by mode interference. Another important reason for using spectrogram zeros is that when the window is the unit Gaussian window, as remarked in [19], STFT admits a Hadamard-Weierstrass decomposition, that can be fully determined by the locations of the spectrogram zeros [22]–[24].

To build our algorithm to localize mode interference in the TF plane, our source of inspiration is the paper by Flandrin [19] in which the properties of the Delaunay triangulation of the zeros of the spectrogram of Gaussian white noises were investigated. Indeed, it was shown in that paper that the edge length in such a triangulation is bounded above by a

maximum value L_e (depending on the normalization of the analysis window), and also that the zeros cannot clutter. Note that a deeper mathematical analysis of the properties of these zeros from the perspective of point processes is available in [20].

B. Localizing Interference Using Delaunay Triangulation of Spectrogram Zeros

In this section, we are going to explain how to use the results of Section III to build an algorithm to localize interference in the TF plane. First, as remarked in [19] the presence of signal in the TF plane gives rise to triangles in the *Delaunay triangulation of spectrogram zeros* (DTSZ) having at least one edge with length exceeding L_e . Then, another interesting remark is that when two modes are interfering the zeros involved in the interference pattern belong to more triangles of that kind than other zeros of the spectrogram. To quantify this, we first propose to keep only the triangles of the DTSZ that contain at least one edge larger than a prescribed threshold. To do so, we sort out the edge lengths in ascending order and then consider the triangles that contain an edge among the P_e % longest, the choice for that parameter being discussed later. At the end of this procedure, we obtain a set of triangles we denote by $\mathcal{T}(P_e)$ from now on. Then we compute the number of such triangles the zeros of the spectrogram belong to by associating with each vertex \mathbf{v} (we use bold notation

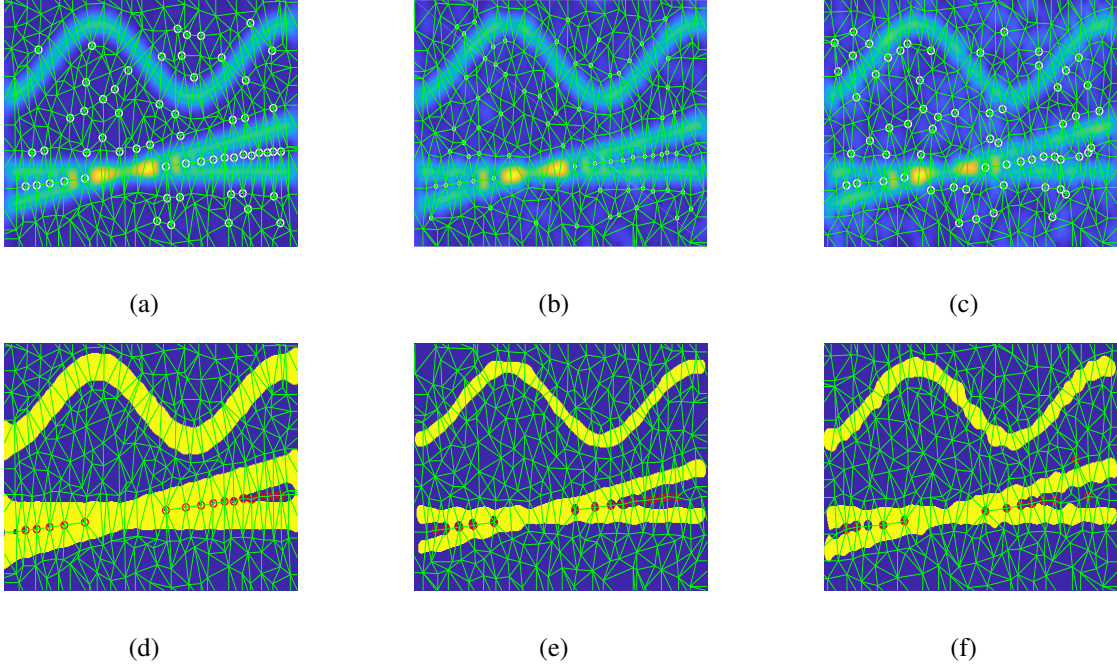


Fig. 4: (a): spectrogram with DTSZ superimposed, the white circles correspond to the zeros \mathbf{v} satisfying $I(\mathbf{v}, 30) \geq 5$ (input SNR equals 20 dB); (b): same as (a) except the input SNR equals 10 dB; (c): same as (a) except the input SNR equals 5 dB; (d): DTSZ on which the mask corresponds to $|V_{\tilde{f}}^g(t, \eta)| \geq \beta\hat{\gamma}$, with $\beta = 8$, the red circles then correspond to $I_{\text{signal}}(\mathbf{v}, 30, 8) = 1$ (input SNR equals 20 dB); (e): same as (d) except the input SNR equals 10 dB; (f): same as (d) except the input SNR equals 5 dB and β is set to 4.

because \mathbf{v} has two components) of the triangulation $\mathcal{T}(P_e)$ a connectivity index as follows:

$$I(\mathbf{v}, P_e) = \#\{T \in \mathcal{T}(P_e), \mathbf{v} \in T\}, \quad (18)$$

where $\#X$ denotes the cardinal of the set X . In this regard, we also define the set of corresponding triangles as follows:

$$\mathcal{T}_{\mathbf{v}}(P_e) = \{T \in \mathcal{T}(P_e), \text{ s.t. } \mathbf{v} \in T\}. \quad (19)$$

To get an insight into what an appropriate value for $I(\mathbf{v}, P_e)$ would be, we consider the two different signals corresponding to the spectrograms depicted in Fig. 3 (a) and (d). In Fig. 3 (a), we superimpose on top of the spectrogram the DTSZ (green edges), the white circles representing the vertices \mathbf{v} such that $I(\mathbf{v}, 30) \geq 1$ (input SNR equals 20 dB). Then, in Fig. 3 (b) and (c), the white circles correspond to $I(\mathbf{v}, 30) \geq 4$ and $I(\mathbf{v}, 30) \geq 5$ respectively. On the second row of Fig. 3, we perform the same computation as that on the first row except we consider the spectrogram of Fig. 3 (d). These first simulations show that the connectivity index is a good parameter to discriminate the zeros associated with interference pattern from the others. The value for P_e has to be chosen all the smaller that more zeros are associated with the signal and finally, by choosing a connectivity index of 5 the zeros associated with interference are kept while many of the other zeros are left apart. In what follows, we denote by "first step" of the algorithm the just described process to select the zeros of the spectrogram.

However, such a simple criterion is not enough to fully

discriminate the zeros associated with interference. To go further, a first naive approach would consist of recalling that, from Section III, the distance between the zeroes located between two interfering pure harmonic modes is monitored by $\frac{1}{\xi_2 - \xi_1}$ so when the modes are close, not only the edges of the triangles crossing the modes should be long, but also the one in the direction of interference is not arbitrary and should larger than L_e when the modes are close. However, as the instantaneous frequencies of the interfering modes are unknown, it is very difficult to build a criterion on that remark and alternatively, we propose to use some information on the energy on the triangles involved in the computation of the connectivity index.

More precisely, consider Φ a zero mean complex Gaussian white noise, then V_{Φ}^g is also Gaussian with zero mean and satisfies:

$$\text{Var}(\Re\{V_{\Phi}^g\}) = \text{Var}(\Im\{V_{\Phi}^g\}) = \sigma^2 \|g\|_2^2, \quad (20)$$

where $\Re\{X\}$ (resp. $\Im\{X\}$) denotes the real (resp. imaginary) part of complex number X , Var the variance, and $\|g\|_2$ is the l_2 norm of the window g . From this, we deduce that $\frac{|V_{\Phi}^g|^2}{\sigma^2 \|g\|_2^2}$ is χ_2 distributed with 2 degrees of freedom. Then, using table of χ_2 law the probability of false alarm is less than 1 % if $|V_{\Phi}^g|$ is larger than $3\sigma \|g\|_2$. So, to separate the noise from the signal in the TF plane, one first computes an estimate of $\gamma = \sigma \|g\|_2$

using the robust estimator proposed in [25], namely:

$$\hat{\gamma} := \frac{\text{median} |\Re \{V_{\tilde{f}}^g\}|}{0.6745}, \quad (21)$$

in which $\tilde{f} = f + \Phi$ denotes the noisy signal.

Based on this analysis of the STFT of the noise, for each vertex selected at the end of the first step, we compute the proportion of triangles involved in the computation of the connectivity index that are above the noise level by computing the following index, for each \mathbf{v} such that $I(\mathbf{v}, P_e) \geq 5$:

$$I_{\text{signal}}(\mathbf{v}, P_e, \beta) = \frac{\#\{T \in \mathcal{T}_{\mathbf{v}}(P_e), \exists(t, \eta) \in T \text{ s.t. } |V_{\tilde{f}}^g(t, \eta)| \geq \beta \hat{\gamma}\}}{\#\mathcal{T}_{\mathbf{v}}(P_e)}. \quad (22)$$

An illustration of the zeros selected using that procedure is given in Fig. 4, when the noise level varies. On the first row, we display the zeros selected by considering $I(\mathbf{v}, 30) \geq 5$ (first step), when the input SNR is equal to 20, 10, and 5 dB, respectively in Fig. 4 (a), (b) and (c). We notice that though some zeros are not associated with interference pattern, the selected set of zeros contain those we want to discriminate. On the second row of Fig. 4, we show that the criterion (22) is very efficient to discriminate the zeros of the interference region from the others. Indeed, in that case, we plot the mask associated with $|V_{\tilde{f}}^g(t, \eta)| \geq \beta \hat{\gamma}$ for an appropriate value for β (yellow zones on Fig. 4. (d), (e) and (f)), the value of which will be discussed later. Then, we select the zeros such that $I_{\text{signal}}(\mathbf{v}, P_e, \beta) = 1$. These correspond to red circles on Fig. 4 (d),(e) and (f), which exactly correspond to the zeros associated with interference. Note that both the zeros associated with TFBs and those associated with more classical interference patterns are detected.

V. PARAMETER DETERMINATION

The algorithm proposed for the determination of the zeros associated with interference depends on three parameters P_e , then the value of $I(\mathbf{v}, P_e)$, and finally β . Our strategy in that matter is to try to discriminate the zeros associated with a single mode from those associated with several modes. In this regard, we remark that, independently of the choice for P_e , the zeros associated with an isolated ridge seldom belong to 5 or more triangles crossing the ridge (such a situation only happens when the ridge has some curvature), so to consider $I(\mathbf{v}, P_e)$ larger or equal to 5 seems a good strategy provided P_e is chosen sufficiently large so as to select only the triangles crossing the ridges when computing the connectivity index. When P_e is small many triangles are associated with noise and then $I(\mathbf{v}, P_e)$ is very often larger or equal to 5, but when P_e increases the number of vertices selected using $I(\mathbf{v}, P_e) \geq 5$ should stabilize and be related to the signal. In Fig. 5 we plot the proportion of zeros kept with respect to P_e assuming $I(\mathbf{v}, P_e) \geq 5$, for the spectrograms of Fig. 4 (a), (b) and (c), corresponding to input SNRs of 20, 10 and 5 dB, respectively. We observe that there exist two different regimes, the first one corresponds to a fast decay of the number of zeros kept and is related to the elimination of the zeros corresponding to noise,

while the smaller decay observed for larger P_e corresponds to the progressive elimination of the zeros associated with the signal. To better illustrate this aspect, we also plot, in Fig. 5, the linear approximation of the data for the different regimes. In this regard, we observe that $P_e = 30$ is a good choice and that the behavior is similar regardless of the noise level.

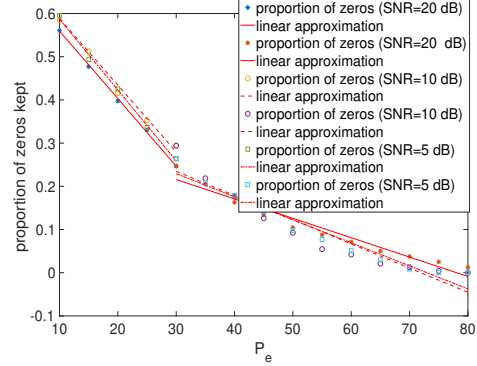


Fig. 5: Proportion of zeros corresponding to $I(\mathbf{v}, P_e) \geq 5$ when P_e varies and for the signal whose spectrograms are depicted in Fig. 4 (a), (b) and (c).

The last parameter we need to fix is β which is used in (22) to fully characterize the zeros associated with interference pattern. To do so, we still consider the spectrograms of Fig. 4 (a), (b) and (c), and that $I(\mathbf{v}, P_e) \geq 5$, and set $P_e = 30$. Of course, this last parameter should be fixed differently depending on the signal. Our strategy to determine the right choice for β is then based on the fact that when β increases the zeros related to noise should be progressively eliminated by considering the vertices \mathbf{v} such that $I_{\text{signal}}(\mathbf{v}, 30, \beta) = 1$. Indeed, when $\beta = 3$, the probability that $|V_{\tilde{f}}^g(t, \eta)| \geq \beta \hat{\gamma}$ at location where only the noise is present is below 1%. In Fig. 6 we compute the number of vertices \mathbf{v} such that

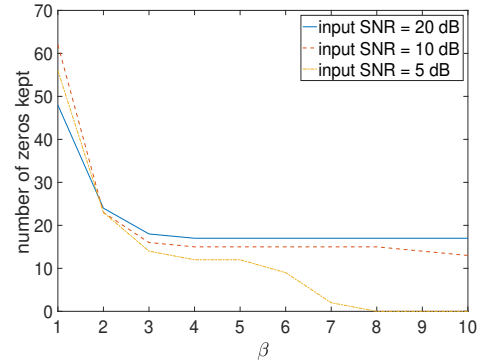


Fig. 6: Number of zeros kept corresponding to $I_{\text{signal}}(\mathbf{v}, 30, \beta) = 1$ when β varies and for the signal whose spectrograms are depicted in Fig. 4 (a), (b) and (c).

$I_{\text{signal}}(\mathbf{v}, 30, \beta) = 1$ with respect to β and again for the spectrogram of Fig. 4 (a), (b) and (c). We notice that, for $\beta \geq 3$, the number of zeros reaches a plateau, this corresponds to all the zeros corresponding to noise have been eliminated,

only remain those of interest. We then notice that these zeros are robust to an increase in the value of β , and all the more so that the noise level is low. In that context, to select the right zeros one should consider a value for β associated with such the plateau regime mentioned above, and thus the possible choices depend on the noise level.

VI. CONCLUSION

In this paper, we first put forward necessary and sufficient conditions for time-frequency bubbles to exist when two parallel pure harmonic modes or linear chirps are interfering. We notice that these conditions are very similar except that the modulation has to be taken into account when considering linear chirps. In the second part of the paper, after noticing that the Delaunay triangulation of spectrogram zeros have very interesting properties, we proposed an algorithm to localize interference in the TF plane based on the analysis of this triangulation. Future work should involve the improvement of the proposed criteria to localize interference regions in heavier noise situations, and it would also certainly be interesting to investigate whether the mathematical characterization of the appearance of TF bubbles could be extended to non parallel modes.

VII. APPENDIX

A. Proof of Proposition III.1

Let us consider the function, $(Ae^{-\pi\sigma^2(\eta-\xi_1)^2} + e^{-\pi\sigma^2(\eta-\xi_2)^2})^2$ whose extrema are the same as those of

$$l(\eta) = Ae^{-\pi\sigma^2(\eta-\xi_1)^2} + e^{-\pi\sigma^2(\eta-\xi_2)^2}.$$

Defining $\xi = \frac{\xi_2 - \xi_1}{2}$ and making the change of variables $\eta = \nu + \frac{\xi_1 + \xi_2}{2}$, we get:

$$l(\nu + \frac{\xi_1 + \xi_2}{2}) = Ae^{-\pi\sigma^2(\nu + \xi)^2} + e^{-\pi\sigma^2(\nu - \xi)^2},$$

which we denote by $q(\nu)$. Differentiating $q(\nu)$, we get after rearranging the terms:

$$\begin{aligned} q'(\nu) &= -2\pi\sigma^2 e^{-\pi\sigma^2(\nu^2 + \xi^2)} \\ &= \left[A(\nu + \xi)e^{-2\pi\sigma^2\xi\nu} + (\nu - \xi)e^{2\pi\sigma^2\xi\nu} \right] \\ &= 2\pi\sigma^2 e^{-\pi\sigma^2\nu^2} e^{-\pi\sigma^2\xi^2} \xi (Ae^{-2\pi\sigma^2\xi\nu} + e^{2\pi\sigma^2\xi\nu}) \\ &\quad \left(-\frac{\nu}{\xi} - \frac{Ae^{-2\pi\sigma^2\xi\nu} - e^{2\pi\sigma^2\xi\nu}}{Ae^{-2\pi\sigma^2\xi\nu} + e^{2\pi\sigma^2\xi\nu}} \right) \quad (23) \\ &= 2\pi\sigma^2 e^{-\pi\sigma^2\nu^2} e^{-\pi\sigma^2\xi^2} \xi (Ae^{-2\pi\sigma^2\xi\nu} + e^{2\pi\sigma^2\xi\nu}) \\ &\quad \left(-\frac{\nu}{\xi} + \tanh(2\pi\sigma^2\xi\nu - \frac{\log(A)}{2}) \right). \end{aligned}$$

So q' has the same sign as $g(\nu) = -\frac{\nu}{\xi} + \tanh(2\pi\sigma^2\xi\nu - \frac{\log(A)}{2})$ whose derivative is:

$$g'(\nu) = \frac{1}{\xi} \left(-1 + 2\pi\sigma^2\xi^2 (1 - \tanh^2(2\pi\sigma^2\xi\nu - \frac{\log(A)}{2})) \right)$$

which is always negative if $2\pi\sigma^2\xi^2 \leq 1$. In such a case, q' is decreasing and then and as $\lim_{\nu \rightarrow -\infty} q'(\nu) = +\infty$ and

$\lim_{\nu \rightarrow +\infty} q'(\nu) = -\infty$, it annihilates once and thus l has a unique extremum which is a maximum.

Now when $2\pi\sigma^2\xi^2 > 1$, g' has two zeros, and we have the following table of variations:

ν	$-\infty$	ν_1	ν_2	$+\infty$
$g'(\nu)$	$-$	0	$+$	0
$g(\nu)$	$+\infty$	\searrow	\nearrow	$-\infty$
		$g(\nu_1)$	$g(\nu_2)$	

If $g(\nu_1) \geq 0$, then $g(\nu)$ and hence $q'(\nu)$ are positive on $]-\infty, \nu_2[$ and $g(\nu)$ and hence $q'(\nu)$ annihilate and change signs at some ν'_2 in $]\nu_2, +\infty[$. In this case, $q(\nu)$ is strictly increasing on $]-\infty, \nu'_2[$ and strictly decreasing on $[\nu'_2, +\infty[$, and thus has a maximum at $\nu = \nu'_2$ which is the unique extremum.

If $g(\nu_2) \leq 0$, $g(\nu)$ and hence $q'(\nu)$ annihilate and change signs once for a certain ν'_1 in $]-\infty, \nu_1[$ and then q has a maximum at $\nu = \nu'_1$ which will be its unique extremum.

If $g(\nu_1) < 0$ and $g(\nu_2) > 0$, $g(\nu)$ and $q'(\nu)$ annihilate and change sign 3 times, once in $]-\infty, \nu_1[$, once in $]\nu_1, \nu_2[$, and once in $[\nu_2, +\infty[$, and thus q has three extrema.

We finally need to compute $g(\nu_1)$ and $g(\nu_2)$. Remember that ν_1 and ν_2 are the roots of g' thus of

$$1 - \frac{1}{2\pi\sigma^2\xi^2} = \tanh^2(2\pi\sigma^2\xi\nu - \frac{\log(A)}{2})$$

and therefore

$$\begin{aligned} \nu_1 &= \frac{1}{2\pi\sigma^2\xi} \left(\frac{\log(A)}{2} + \operatorname{arctanh}\left(-\sqrt{1 - \frac{1}{2\pi\sigma^2\xi^2}}\right) \right) \\ \nu_2 &= \frac{1}{2\pi\sigma^2\xi} \left(\frac{\log(A)}{2} + \operatorname{arctanh}\left(\sqrt{1 - \frac{1}{2\pi\sigma^2\xi^2}}\right) \right) \end{aligned}$$

and thus as $\alpha = \sqrt{\frac{\pi}{2}}\sigma(\xi_2 - \xi_1) = \sqrt{2\pi}\sigma\xi$, we may write:

$$\begin{aligned} g(\nu_1) &= -\frac{\log(A)}{4\pi\sigma^2\xi^2} - \frac{\operatorname{arctanh}\left(-\sqrt{1 - \frac{1}{2\pi\sigma^2\xi^2}}\right)}{2\pi\sigma^2\xi^2} \\ &\quad - \sqrt{1 - \frac{1}{2\pi\sigma^2\xi^2}} \\ &= -\frac{\log(A)}{2\alpha^2} - \frac{\operatorname{arctanh}\left(-\frac{\sqrt{\alpha^2-1}}{\alpha}\right)}{\alpha^2} - \frac{\sqrt{\alpha^2-1}}{\alpha} \\ &= -\frac{\log(A)}{2\alpha^2} - \frac{\log\left(\frac{\alpha-\sqrt{\alpha^2-1}}{\alpha+\sqrt{\alpha^2-1}}\right)}{2\alpha^2} - \frac{\sqrt{\alpha^2-1}}{\alpha} \\ g(\nu_2) &= -\frac{\log(A)}{2\alpha^2} - \frac{\log\left(\frac{\alpha+\sqrt{\alpha^2-1}}{\alpha-\sqrt{\alpha^2-1}}\right)}{2\alpha^2} + \frac{\sqrt{\alpha^2-1}}{\alpha}. \end{aligned}$$

From this we deduce that $g(\nu_1) < 0$ and $g(\nu_2) > 0$, and thus q has three extrema, if and only if:

$$|\log(A)| < 2\alpha\sqrt{\alpha^2-1} - \log\left(\frac{\alpha+\sqrt{\alpha^2-1}}{\alpha-\sqrt{\alpha^2-1}}\right).$$

B. Proof of Proposition III.2

The derivative of $|V_f^h(\tilde{t}_k, \eta)|^2$ is null if η satisfies:

$$\begin{aligned} &\left((\xi_1 - \eta)Ae^{-\pi\sigma^2(\eta-\xi_1)^2} + (\eta - \xi_2)e^{-\pi\sigma^2(\eta-\xi_2)^2} \right) \\ &\quad \left(Ae^{-\pi\sigma^2(\eta-\xi_1)^2} - e^{-\pi\sigma^2(\eta-\xi_2)^2} \right) = 0. \end{aligned} \quad (24)$$

Looking for a a solution in $[\xi_1, \xi_2]$, we remark that the derivative is null if $Ae^{-\pi\sigma^2(\eta-\xi_1)^2} - e^{-\pi\sigma^2(\eta-\xi_2)^2} = 0$, which leads to

$$\hat{\eta} = \frac{\log A}{2\pi\sigma^2(\xi_1 - \xi_2)} + \frac{\xi_1 + \xi_2}{2}. \quad (25)$$

This extremum corresponds to a zero of $|V_f^h(\tilde{t}_k, \eta)|^2$, and is thus a minimum of $|V_f^h(\tilde{t}_k, \eta)|^2$. Now, considering the same formalism as previously, outside of the interval $]\xi_1, \xi_2[$, the extrema satisfy

$$\frac{\eta - \xi_1}{\eta - \xi_2} = Ae^{-2\pi\sigma^2(\xi_1 - \xi_2)(\eta - \frac{\xi_1 + \xi_2}{2})}. \quad (26)$$

Putting $h_1(\eta) = \frac{\eta - \xi_1}{\eta - \xi_2}$ and $h_2(\eta) = Ae^{-2\pi\sigma^2(\xi_1 - \xi_2)(\eta - \frac{\xi_1 + \xi_2}{2})}$, we remark that $h_1'(\eta) < 0$ and $h_2'(\eta) > 0$. On interval $]-\infty, \xi_1[$, as $\lim_{\eta \rightarrow -\infty} h_1(\eta) = 1$, $h_1(\xi_1) = 0$, $\lim_{\eta \rightarrow -\infty} h_2(\eta) = 0$ and $h_2(\xi_1) = Ae^{-\pi\sigma^2(\xi_1 - \xi_2)^2}$, so there is a unique solution to (26) in $]-\infty, \xi_1[$, corresponding to a maximum for $|V_f^h(\tilde{t}_k, \eta)|^2$. Investigating the case of interval $]\xi_2, +\infty[$, as $\lim_{\eta \rightarrow \xi_2} h_1(\eta) = +\infty$, $\lim_{\eta \rightarrow +\infty} h_1(\eta) = 1$, $h_2(\xi_2) = Ae^{\pi\sigma^2(\xi_2 - \xi_1)^2}$ and $\lim_{\eta \rightarrow +\infty} h_2(\eta) = +\infty$ there is a unique solution to (26) in $]\xi_2, +\infty[$, which corresponds to a maximum for $|V_f^h(\tilde{t}_k, \cdot)|^2$.

C. Proof of Proposition III.3

Let us consider $A = 1$, for which we put:

$$l(\eta) = e^{-2\pi\sigma^2(\eta-\xi_1)^2} + e^{-2\pi\sigma^2(\eta-\xi_2)^2} + 2e^{-\pi\sigma^2[(\eta-\xi_1)^2 + (\eta-\xi_2)^2]} \cos(2\pi(\xi_2 - \xi_1)t), \quad (27)$$

and then define $\gamma = \cos(2\pi(\xi_2 - \xi_1)t)$. Considering the same change of variables as previously, namely $\eta = \nu + \frac{\xi_1 + \xi_2}{2}$ and relling $\xi = \frac{\xi_2 - \xi_1}{2}$, we define:

$$\begin{aligned} q(\nu) &:= l\left(\nu + \frac{\xi_1 + \xi_2}{2}\right) \\ &= e^{-2\pi\sigma^2(\nu+\xi)^2} + e^{-2\pi\sigma^2(\nu-\xi)^2} \\ &\quad + 2e^{-\pi\sigma^2[(\nu+\xi)^2 + (\nu-\xi)^2]} \gamma, \end{aligned} \quad (28)$$

whose derivative reads:

$$\begin{aligned} q'(\nu) &= 8\pi\sigma^2 e^{-2\pi\sigma^2\nu^2} e^{-2\pi\sigma^2\xi^2} \\ &\quad [-\nu(\cosh(4\pi\sigma^2\xi\nu) + \gamma) + \xi \cosh(4\pi\sigma^2\xi\nu)] \\ &= 8\pi\sigma^2 e^{-2\pi\sigma^2\nu^2} e^{-2\pi\sigma^2\xi^2} (\cosh(4\pi\sigma^2\xi\nu) + \gamma) \\ &\quad \left[-\nu + \xi \frac{\sinh(4\pi\sigma^2\xi\nu)}{\cosh(4\pi\sigma^2\xi\nu) + \gamma} \right], \end{aligned} \quad (29)$$

which has the sign of the odd function $k(\nu) = -\nu + \xi \frac{\sinh(4\pi\sigma^2\xi\nu)}{\cosh(4\pi\sigma^2\xi\nu) + \gamma}$ (so we study it only for positive ν). Computing the derivative of this function we get:

$$\begin{aligned} k'(\nu) &= -1 + 4\pi\sigma^2\xi^2 \\ &\quad \frac{\cosh(4\pi\sigma^2\xi\nu)(\cosh(4\pi\sigma^2\xi\nu) + \gamma) - \sinh^2(4\pi\sigma^2\xi\nu)}{(\cosh(4\pi\sigma^2\xi\nu) + \gamma)^2} \\ &= -1 + 4\pi\sigma^2\xi^2 \frac{1 + \beta \cosh(4\pi\sigma^2\xi\nu)}{(\cosh(4\pi\sigma^2\xi\nu) + \gamma)^2}, \end{aligned} \quad (30)$$

which has the same sign as

$$r(\nu) = -(\cosh(4\pi\sigma^2\xi\nu) + \gamma)^2 + 4\pi\sigma^2\xi^2(1 + \gamma \cosh(4\pi\sigma^2\xi\nu)).$$

Differentiating again, we get

$$\begin{aligned} r'(\nu) &= -2(\cosh(4\pi\sigma^2\nu\xi) + \gamma)4\pi\sigma^2 \sinh(4\pi\sigma^2\nu\xi) \\ &\quad + 16\pi^2\xi^3\sigma^4\xi^2 \sinh(4\pi\sigma^2\nu\xi) \\ &= 8\pi\xi\sigma^2 \sinh(4\pi\sigma^2\nu\xi) \\ &\quad (-\cosh(4\pi\sigma^2\nu\xi) - \gamma + 2\pi\sigma^2\xi^2). \end{aligned} \quad (31)$$

which has the sign of $s(\nu) = -\cosh(4\pi\sigma^2\nu\xi) - \gamma + 2\pi\sigma^2\xi^2$ which is decreasing for $\nu > 0$. As $s(0) = -1 - \gamma + 2\pi\sigma^2\xi^2$, we have two cases. The first one is when $-1 - \gamma + 2\pi\sigma^2\xi^2 \leq 0$. As $r(0) = -(1 + \gamma)^2 + 4\pi\sigma^2\xi^2(1 + \gamma) = (1 + \alpha)(-1 - \gamma + 4\pi\sigma^2\xi^2)$, if $-1 - \gamma + 4\pi\sigma^2\xi^2 \leq 0$, we have the following table of variations:

ν	0	$+\infty$
$r'(\nu)$		-
$r(\nu)$	$r(0) \leq 0$	$-\infty$
$k'(\nu)$		-
$k(\nu)$	0	$-\infty$

Note that from the above table of variations we deduce that the function q is decreasing for $\nu > 0$, and q has a unique maximum at 0. Now if $-1 - \gamma + 4\pi\sigma^2\xi^2 > 0$ still with $-1 - \gamma + 2\pi\sigma^2\xi^2 \leq 0$, we get the table of variations:

ν	0	ν_0	ν_1	ν_2	$+\infty$
$r'(\nu)$			-		
$r(\nu)$	$r(0) > 0$				$-\infty$
$k'(\nu)$		+	0	-	
$k(\nu)$	0				$-\infty$
$q'(\nu)$		+	0	-	
$q(\nu)$	$q(0)$				$-\infty$

and so in that case, we obtain that q has three extrema.

The second case corresponds to $-1 - \gamma + 2\pi\sigma^2\xi^2 > 0$, then $-1 - \gamma + 4\pi\sigma^2\xi^2 > 0$ then $r(0) > 0$, and we get the following table of variations:

ν	0	ν_0	ν_1	ν_2	$+\infty$
$r'(\nu)$		+	0	-	
$r(\nu)$	$r(0) > 0$				$-\infty$
$k'(\nu)$		+	0	-	
$k(\nu)$	0				$-\infty$
$q'(\nu)$		+	0	-	
$q(\nu)$	$q(0)$				$-\infty$

Conclusion: The function q has three extrema if $1 + \gamma < 4\pi\sigma^2\xi^2$, which corresponds to the sought condition, and 1 otherwise.

D. Proof of Proposition III.4

Let us consider the function:

$$l(\eta) = A^2 e^{-2\pi\sigma^2(\eta-\xi_1)^2} + e^{-2\pi\sigma^2(\eta-\xi_2)^2} + 2Ae^{-\pi\sigma^2[(\eta-\xi_1)^2+(\eta-\xi_2)^2]} \cos(2\pi(\xi_2 - \xi_1)t), \quad (32)$$

and then put $\gamma = \cos(2\pi(\xi_2 - \xi_1)t)$ Considering the same change of variables as previously, namely $\eta = \nu + \frac{\xi_1 + \xi_2}{2}$ and putting $\xi = \frac{\xi_2 - \xi_1}{2}$, we may write:

$$f_1(\nu) = l\left(\nu + \frac{\xi_1 + \xi_2}{2}\right) = e^{-2\pi\sigma^2(\nu^2 + \xi^2)} (A^2 e^{-4\pi\sigma^2\xi\nu} + e^{4\pi\sigma^2\xi\nu} + 2A\gamma). \quad (33)$$

We then make a new change of variables by putting $\nu = \frac{\log(A) + \mu}{4\pi\sigma^2\xi}$, which enables us to write:

$$f_1(\nu) = f_2(\mu) = e^{-2\pi\sigma^2 \left[\left(\frac{\log(A) + \mu}{4\pi\sigma^2\xi} \right)^2 + \xi^2 \right]} (Ae^{-\mu} + Ae^{\mu} + 2A\gamma) \quad (34)$$

$$= e^{-2\pi\sigma^2 \left[\left(\frac{\log(A) + \mu}{4\pi\sigma^2\xi} \right)^2 + \xi^2 \right]} 2As(\cosh(\mu) + \gamma).$$

The derivative of f_2 reads:

$$f_2'(\mu) = e^{-2\pi\sigma^2 \left[\left(\frac{\log(A) + \mu}{4\pi\sigma^2\xi} \right)^2 + \xi^2 \right]} 2A \left[-\frac{\log(A) + \mu}{4\pi\sigma^2\xi^2} (\cosh(\mu) + \gamma) + \sinh(\mu) \right] \quad (35)$$

which has the sign of:

$$g(\mu) = -\frac{\log(A) + \mu}{4\pi\sigma^2\xi^2} + \frac{\sinh(\mu)}{\cosh(\mu) + \gamma}$$

assuming $\gamma \neq -1$, and recalling that $\alpha = \sqrt{\frac{\pi}{2}}\sigma(\xi_2 - \xi_1) = \sqrt{2\pi}\sigma\xi$, we rewrite:

$$g(\mu) = -\frac{\log(A) + \mu}{2\alpha^2} + \frac{\sinh(\mu)}{\cosh(\mu) + \gamma}.$$

Differentiating g we get

$$g'(\mu) = -\frac{1}{2\alpha^2} + \frac{\cosh(\mu)(\cosh(\mu) + \gamma) - \sinh^2(\mu)}{(\cosh(\mu) + \gamma)^2} \quad (36)$$

$$= -\frac{1}{2\alpha^2} + \frac{1 + \gamma \cosh(\mu)}{(\cosh(\mu) + \gamma)^2}$$

which has the same sign as

$$h(\cosh(\mu)) = -\frac{(\cosh(\mu) + \gamma)^2}{2\alpha^2} + 1 + \gamma \cosh(\mu)$$

$$= -\frac{\cosh(\mu)^2}{2\alpha^2} + \gamma\left(1 - \frac{1}{\alpha^2}\right) \cosh(\mu) + 1 - \frac{\gamma^2}{2\alpha^2}$$

$$= \frac{1}{\alpha^2} \left(-\frac{\cosh(\mu)^2}{2} + \gamma(\alpha^2 - 1) \cosh(\mu) + \alpha^2 - \frac{\gamma^2}{2} \right).$$

The term inside the parentheses is a second order polynomial in $\cosh(\mu)$ whose discriminant reads:

$$\Delta = \gamma^2(\alpha^2 - 1)^2 + (2\alpha^2 - \gamma^2) = \alpha^2(\gamma^2(\alpha^2 - 2) + 2) > 0.$$

The roots of this polynomial are denoted by X_1 and X_2 with $X_1 < X_2$, and we know that $h(X) < 0$ if $X \in$

$] -\infty, X_1[\cup] X_2, +\infty[$ and $h(X) > 0$ if $X \in] X_1, X_2[$.

We now need to know the location of $\cosh(\mu)$. To do this, let us first compute $h(1) = (\gamma + 1)(1 - \frac{\gamma+1}{2\alpha^2})$ which has the same sign as $\alpha^2 - \frac{\gamma+1}{2}$. Let us assume $\alpha \leq \sqrt{\frac{\gamma+1}{2}}$, as $h(1) \leq 0$ then 1 belongs to $] -\infty, X_1[$ or $] X_2, +\infty[$. To determine to which interval 1 belongs to we compare it to $\frac{X_1 + X_2}{2} = \gamma(\alpha^2 - 1) < 1$. Thus 1 belongs to $] X_2, +\infty[$. Finally, as for all $\mu \in \mathbb{R}$ $\cosh(\mu) \geq 1$, $h(\mu)$ and thus $g'(\mu)$ are negative. From this study we deduce the following table of variations:

μ	$-\infty$	μ_1	$+\infty$	
$g(\mu)$	$+\infty$	↘		$-\infty$
$f_2'(\mu)$	+		0	-
$f_2(\mu)$	↗		↘	

and that the function $l(\eta)$ has a unique extremum which is a maximum when $\alpha \leq \sqrt{\frac{\gamma+1}{2}}$.

If we now assume that $\alpha > \sqrt{\frac{\gamma+1}{2}}$, then $h(1) > 0$ and thus 1 belongs to $] X_1, X_2[$. As $\cosh(\mu) \in] X_1, X_2[$ is equivalent to $|\mu| < \text{arccosh}(X_2)$, this means that $h(\cosh(\mu)) < 0$ if

$$\mu \in] -\infty, -\text{arccosh}(X_2)[\cup] \text{arccosh}(X_2), +\infty[,$$

and $h(\cosh(\mu))$ is positive in the opposite case. We thus get the following table of variations:

μ	$-\infty$	$-\text{arccosh}(X_2)$	$\text{arccosh}(X_2)$	$+\infty$	
$g'(\mu)$	-		+	0	-
$g(\mu)$	$+\infty$	↗ ↘		$-\infty$	

$g(\mu)$ vanishes with a change of sign only once at some $\mu = \mu_1$ if and only if $g(-\text{arccosh}(X_2)) \geq 0$ or $g(\text{arccosh}(X_2)) \leq 0$. In this case, we deduce that

μ	$-\infty$	μ_1	$+\infty$
$f_2'(\mu)$	+		-
$f_2(\mu)$	↗		↘

meaning $l(\eta)$ has a unique maximum in that case (which is a maximum).

If $g(-\text{arccosh}(X_2)) < 0$ and $g(\text{arccosh}(X_2)) > 0$, $g(\mu)$ will vanish with a change of signs three times at some $\mu = \mu_1, \mu_2$ and μ_3 respectively. We therefore deduce the following table of variations for f_2 :

μ	$-\infty$	μ_1	μ_2	μ_3	$+\infty$	
$g(\mu)$	+		0	+	0	-
$f_2(\mu)$	↗		↘	↗	↘	

In such case, $l(\eta)$ has three extrema: 2 maxima and a minimum.

Finally, to specify in which situations l has three extrema, as

$$g(\text{arccosh}(X_2)) = -\frac{\log(A) + \text{arccosh}(X_2)}{2\alpha^2} + \frac{\sqrt{X_2^2 - 1}}{X_2 + \gamma}$$

$$g(-\text{arccosh}(X_2)) = -\frac{\log(A) - \text{arccosh}(X_2)}{2\alpha^2} - \frac{\sqrt{X_2^2 - 1}}{X_2 + \gamma}$$

we deduce that:

$$\begin{aligned} g(\operatorname{arccosh}(X_2)) &> 0 \\ \Leftrightarrow \log(A) &< -\operatorname{arccosh}(X_2) + 2\alpha^2 \frac{\sqrt{X_2^2 - 1}}{X_2 + \gamma} \\ g(-\operatorname{arccosh}(X_2)) &< 0 \\ \Leftrightarrow -\log(A) &< -\operatorname{arccosh}(X_2) + 2\alpha^2 \frac{\sqrt{X_2^2 - 1}}{X_2 + \gamma}. \end{aligned} \quad (37)$$

From this we get that $l(\eta)$ has three extrema if and only if $\alpha > \sqrt{\frac{1+\gamma}{2}}$ and then if $|\log(A)| < -\operatorname{arccosh}(X_2) + 2\alpha^2 \frac{\sqrt{X_2^2 - 1}}{X_2 + \alpha}$ with $X_2 = \gamma(\alpha^2 - 1) + \alpha\sqrt{\gamma^2(\alpha^2 - 2) + 2}$.

E. Proof of Proposition III.5

In this section, we assume that $-1 < \gamma \leq 1$. We know that $f_2'(\mu)$ has the same sign as:

$$g(\mu) = -\frac{\log(A) + \mu}{4\pi\sigma^2\xi^2} + \frac{\sinh(\mu)}{\cosh(\mu) + \gamma}$$

we denote this function by $g(\mu, \gamma)$. We can rewrite:

$$g(\mu, \gamma) = -\frac{\log(A) + \mu}{2\alpha^2} + \frac{\sinh(\mu)}{\cosh(\mu) + \gamma}.$$

We know from the previous proposition that the function f_2 has three extrema if and only if

$$\alpha > \sqrt{\frac{1+\gamma}{2}} \text{ and}$$

$$g(-\operatorname{arccosh}(X_2), \gamma) < 0 \text{ and } g(\operatorname{arccosh}(X_2), \gamma) > 0$$

Let us show that this is equivalent to:

$$\exists y_0 < 0 \ g(y_0, \gamma) < 0 \text{ and } y_0' > 0 \ g(y_0', \gamma) > 0$$

This condition is a necessary condition since the values $y_0 = -\operatorname{arccosh}(X_2)$ and $y_0' = \operatorname{arccosh}(X_2)$, satisfy the property. Conversely, let us assume that there exist $y_0 < 0$ and $y_0' > 0$ such that $g(y_0, \gamma) < 0$ and $g(y_0', \gamma) > 0$. As $\lim_{\mu \rightarrow +\infty} g(\mu, \gamma) = -\infty$ and $\lim_{\mu \rightarrow -\infty} g(\mu, \gamma) = +\infty$, this implies that $g(\cdot, \gamma)$ (and also $f_2'(\mu)$) passes through 0 and changes signs three times, respectively on the intervals $]-\infty, y_0[$, $]y_0, y_0'[$, and on $]y_0', +\infty[$, and thus f_2 has three extrema.

Let us now show that, if the function f_2 has three extrema for $\gamma = 1$, it also has three extrema for $\gamma \in]-1, 1[$. Based on the above characterization of the existence of three extrema based on the study of the function g , let us assume that there exist $y_0 < 0$ and $y_0' > 0$ such that $g(y_0, 1) < 0$ and $g(y_0', 1) > 0$. But whatever $\gamma \in]-1, 1[$ one has $\forall \mu \in \mathbb{R} \ \frac{1}{\cosh(\mu)} \geq \frac{1}{\cosh(\mu)+1}$, which means that

$$\begin{aligned} \forall \mu \geq 0, \quad \frac{\sinh(\mu)}{\cosh(\mu) + \gamma} &\geq \frac{\sinh(\mu)}{\cosh(\mu) + 1} \text{ and} \\ \forall \mu \leq 0, \quad \frac{\sinh(\mu)}{\cosh(\mu) + \gamma} &\leq \frac{\sinh(\mu)}{\cosh(\mu) + 1}. \end{aligned}$$

Finally, we deduce that

$$\forall \mu \geq 0, \ g(\mu, \gamma) \geq g(\mu, 1) \text{ and } \forall \mu \leq 0, \ g(\mu, \gamma) \leq g(\mu, 1).$$

This means in particular that $g(y_0', \gamma) \geq g(y_0', 1)$, and that $g(y_0, \gamma) \leq g(y_0, 1)$. So we deduce from this that $g(y_0', \gamma) > 0$

and $g(y_0, \gamma) < 0$, and thus whatever $\gamma \in]-1, 1[$, the function g satisfies the condition for f_2 to have three extrema.

So finally, we may conclude that the function f_2 has three extrema whatever $\gamma \in]-1, 1[$, if and only if

$$\alpha > 1 \text{ and } |\log(A)| < -2\operatorname{arccosh}(\alpha) + 2\alpha\sqrt{\alpha^2 - 1}.$$

REFERENCES

- [1] N. Delprat, B. Escudié, P. Guillemain, R. Kronland-Martinet, P. Tchamitchian, and B. Torresani, "Asymptotic wavelet and gabor analysis: Extraction of instantaneous frequencies," *IEEE transactions on Information Theory*, vol. 38, no. 2, pp. 644–664, 1992.
- [2] P. Flandrin, *Time-frequency/time-scale analysis*. Academic Press, 1998, vol. 10.
- [3] L. Stankovic, M. Dakovic, and V. Ivanovic, "Performance of spectrogram as IF estimator," *Electronics Letters*, vol. 37, no. 12, pp. 797–799, 2001.
- [4] R. Carmona, W. Hwang, and B. Torresani, "Multiridge detection and time-frequency reconstruction," *IEEE Transactions on Signal Processing*, vol. 47, no. 2, pp. 480–492, Feb 1999.
- [5] R. G. Baraniuk, P. Flandrin, A. J. Janssen, and O. J. Michel, "Measuring time-frequency information content using the Rényi entropies," *IEEE Transactions on Information theory*, vol. 47, no. 4, pp. 1391–1409, 2001.
- [6] S. Meignen, M. Colominas, and D.-H. Pham, "On the use of Rényi entropy for optimal window size computation in the short-time Fourier transform," in *ICASSP 2020-2020 IEEE International Conference on Acoustics, Speech and Signal Processing (ICASSP)*. IEEE, 2020, pp. 5830–5834.
- [7] H. K. Kwok and D. L. Jones, "Improved instantaneous frequency estimation using an adaptive short-time fourier transform," *IEEE transactions on signal processing*, vol. 48, no. 10, pp. 2964–2972, 2000.
- [8] J. Zhong and Y. Huang, "Time-frequency representation based on an adaptive short-time fourier transform," *IEEE Transactions on Signal Processing*, vol. 58, no. 10, pp. 5118–5128, 2010.
- [9] L. Li, H. Cai, and Q. Jiang, "Adaptive synchrosqueezing transform with a time-varying parameter for non-stationary signal separation," *Applied and Computational Harmonic Analysis*, 2019.
- [10] L. Li, H. Cai, H. Han, Q. Jiang, and H. Ji, "Adaptive short-time Fourier transform and synchrosqueezing transform for non-stationary signal separation," *Signal Processing*, vol. 166, p. 107231, 2020.
- [11] F. Auger and P. Flandrin, "Improving the readability of time-frequency and time-scale representations by the reassignment method," *IEEE Transactions on Signal Processing*, vol. 43, no. 5, pp. 1068–1089, 1995.
- [12] V. Bruni, M. Tartaglione, and D. Vitulano, "On the time-frequency reassignment of interfering modes in multicomponent FM signals," in *2018 26th European Signal Processing Conference (EUSIPCO)*. IEEE, 2018, pp. 722–726.
- [13] —, "A fast and robust spectrogram reassignment method," *Mathematics*, vol. 7, no. 4, p. 358, 2019.
- [14] I. Reinhold, M. Sandsten, and J. Starkhammar, "Objective detection and time-frequency localization of components within transient signals," *The Journal of the Acoustical Society of America*, vol. 143, no. 4, pp. 2368–2378, 2018.
- [15] J. Brynolfsson, I. Reinhold, J. Starkhammar, and M. Sandsten, "The matched reassignment applied to echolocation data," in *ICASSP 2019-2019 IEEE International Conference on Acoustics, Speech and Signal Processing (ICASSP)*. IEEE, 2019, pp. 8236–8240.
- [16] J. Xiao and P. Flandrin, "Multitaper time-frequency reassignment for nonstationary spectrum estimation and chirp enhancement," *IEEE Transactions on Signal Processing*, vol. 55, no. 6, pp. 2851–2860, June 2007.
- [17] M. Sandsten, I. Reinhold, and R. Anderson, "A multitaper reassigned spectrogram for increased time-frequency localization precision," in *ICASSP 2020-2020 IEEE International Conference on Acoustics, Speech and Signal Processing (ICASSP)*. IEEE, 2020, pp. 5310–5314.
- [18] N. Delprat, "Global frequency modulation laws extraction from the gabor transform of a signal: A first study of the interacting components case," *IEEE transactions on speech and audio processing*, vol. 5, no. 1, pp. 64–71, 1997.
- [19] P. Flandrin, "Time-frequency filtering based on spectrogram zeros," *IEEE Signal Processing Letters*, vol. 22, no. 11, pp. 2137–2141, 2015.
- [20] R. Bardenet, J. Flamant, and P. Chainais, "On the zeros of the spectrogram of white noise," *Applied and Computational Harmonic Analysis*, vol. 48, no. 2, pp. 682–705, 2020.

- [21] S. Meignen, T. Oberlin, P. Depalle, P. Flandrin, and S. McLaughlin, "Adaptive multimode signal reconstruction from time–frequency representations," *Philosophical Transactions of the Royal Society A: Mathematical, Physical and Engineering Sciences*, vol. 374, no. 2065, p. 20150205, 2016.
- [22] R. P. Boas, *Entire functions*. Academic Press, 2011.
- [23] K. Gröchenig, *Foundations of time-frequency analysis*. Springer Science & Business Media, 2001.
- [24] H. Korsch, C. Müller, and H. Wiescher, "On the zeros of the husimi distribution," *Journal of Physics A: Mathematical and General*, vol. 30, no. 20, p. L677, 1997.
- [25] D. Donoho and I. Johnstone, "Ideal spatial adaptation via wavelet shrinkage," *Biometrika*, vol. 81, pp. 425–455, 1994.